Journal of Bionic Engineering (2023) 20:934–952
https://doi.org/10.1007/s42235-022-00328-4

Design and Mechanics of a Composite Wave-driven Soft Robotic Fin for Biomimetic Amphibious Robot

Minghai Xia[1] · He Wang[1] · Qian Yin[1,2] · Jianzhong Shang[1] · Zirong Luo[1] · Qunwei Zhu[1]

Received: 17 August 2022 / Revised: 8 December 2022 / Accepted: 9 December 2022 / Published online: 27 January 2023

Abstract
Bionic amphibious robots have important prospects in scientific, commercial, and military fields. Compared with traditional amphibious robots which use propellers/jets for aquatic medium and wheels/tracks for terrestrial medium, bionic propulsion method has great advantages in terms of manoeuvrability, efficiency, and reliability, because there is no need to switch between different propulsion systems. To explore the integrated driving technology of amphibious robot, a novel bio-inspired soft robotic fin for amphibious use is proposed in this paper. The bionic fin can swim underwater and walk on land by the same undulating motion. To balance the conflicting demands of flexibility underwater and rigidity on land, the undulating fin adopts a special combination of a membrane fin and a bending spring. A periodic longitudinal wave in horizontal direction has been found generating passively in dynamic analysis. To find the composite wave-driven mechanics, theoretical analysis is conducted based on the walking model and swimming model. A virtual prototype is built in ADAMS software to verify the walking mechanics. The simulation result reveals that the passive longitudinal wave is also periodical and the composite wave contributes to land walking. Finally, an amphibious robot prototype actuated by a pair of undulating fins has been developed. The experiments show that the robot can achieve multiple locomotion, including walking forward/backward, turning in place, swimming underwater, and crossing medium, thus giving evidence to the feasibility of the newly designed undulating fin for amphibious robot.

Keywords Undulating fin · Amphibious robot · Composite wave driven · Locomotion mechanism

1 Introduction

In the past 20 years, amphibious robots have attracted much attention of researchers and represented growing development due to their outstanding advantages in unstructured and complex environment [1]. Compared with robots which can only work in neither aquatic nor terrestrial mediums, amphibious robots have been proved to be more flexible, adaptive, and robust [2]. Owning to these prominent merits, amphibious robots have wide application prospects in scientific, commercial, and military fields, such as reconnaissance, offshore mine detection, disaster rescue, water quality monitoring, and ecosystem protection [1, 3, 4].

Propulsion system is the main difficulty for the application of amphibious robot because of the huge difference in land and water environment. The main propulsion way for Unmanned Ground Vehicles (UGVs) includes wheels and tracks. And Unmanned Underwater Vehicles (UUVs) usually use propellers and water jets [5]. As traditional driven systems above are only suitable for single medium, it is worthwhile to find a united driving mechanism so as to reduce structure complexity and enhance system reliability. Bionic amphibious robots, which gain inspiration from natural creatures, especially amphibians [6], have become the solution for this problem. In the past years, different bionic amphibious robot have been introduced based to their biological prototypes, including (1) bionic cockroach [7–11], (2) bionic crab [12–14], (3) bionic lobster [15], (4) bionic turtle [16–18], (5) bionic salamander [19], (6) bionic frog

✉ Jianzhong Shang
shangjianzhong@nudt.edu.cn

✉ Zirong Luo
luozirong@nudt.edu.cn

[1] College of Intelligence Science and Technology, National University of Defense Technology, Changsha 410073, China

[2] College of Energy and Power Engineering, Changsha University of Science and Technology, Changsha 410076, China

[20], (7) bionic sea urchin [21], (8) bionic snake [22, 23], (9) bionic fish [24, 25], etc.

In those bionic prototypes, snakes and fishes are distinguished with others, because they are moving by undulating motion instead of legs or crawling feet. Snakes present high speed, agile locomotion, strong adaptivity, and obstacle-climbing capability by the swing of bodies; and fishes also have excellent three-dimensional manoeuvrability under water by undulating their bodies and fins. Based on the propulsive patterns, fishes have two swimming modes: (1) Body and/or Caudal Fin (BCF) propulsion and (2) Medium and/or Paired Fin (MPF) propulsion [26]. BCF propeller generates driven force by oscillating the caudal fin or bending the body. By contrast, MPF-propelled fish propagate travelling waves by undulating long medium or pectoral fins so as to generate thrust. It can be observed that the locomotion of undulating fins and snakes are quite similar. Therefore, using combined bionic approach, undulating fin can be expanded as the propulsion component of amphibious robot.

At present, the research of bionic undulating fin for aquatic medium is relatively mature. Due to the advantage of high manoeuvrability and low-speed stability, biomimetic underwater robots based on MPF propulsion have been developed over the world [27–32]. In 2018, the Office of Naval Research (ONR) and Pliant Energy System of US designed a new amphibious robot Velox [25], which can swim underwater and walk on ground by a pair of ribbon fins. Owning to the flexible and united propulsion system, Velox can also adapt to complex environment, including walking on smooth ice and sand roads as well as swimming on seabed, which shows that MPF-inspired undulatory propulsion has outstanding prospects for amphibious robots.

However, the undulating fins of Velox are specially made and they are very thick so as to support the robot body on land, which sacrifices the flexibility of the fin and increase the weight. Besides, it is hard to find a proper material for amphibious fins. In early explorations, researchers have used different materials to fabricate bionic fin, including nitrile rubber [33], silicone rubber [34, 35], rubber [36], Lycra [32], and so on. However, they are all used underwater where elasticity, weight, and permeability are the main considerations. When it comes to terrestrial robot, the fin is supposed to have adequate bending capacity so as to support the robot body and maintain a complete wave, in which case the fin should be as thick as possible. Unfortunately, it is accompanied with excessive weight and heavy load on motors, resulting in huge resistance and energy consumption.

To find a lightweight design method and reduce material cost, we have designed a novel robotic undulating fin for amphibious robot, as shown in Fig. 1. The flexible fin is strengthened with a rigid bending spring so as to balance the demands of flexibility underwater and rigidity on land. As traditional fin rays that clamp the flexible fin can only oscillate up and down, we have designed a self-adaptive fin ray that has two additional passive rotational degrees of freedom for improvement. When the active transverse wave propagates, a longitudinal wave is found generating passively due to the interaction of the fin rays and the spring. This composite wave is quietly different from the traditional bionic waveform that consists of only one-dimensional wave. It is worthwhile to find the locomotion mechanism of the composite wave and give further suggestion for amphibious fin design.

The rest of the paper is organized as follows. Section 2 presents the mechanical design of the undulating fin and the composite wave-driven mechanics in land/water media. The simulation for the walking model is conducted and discussed in Sect. 3. In Sect. 4, an amphibious robot prototype based on a pair of the novel undulating fin is introduced and locomotion experiments are conducted. The research results are discussed in Sect. 5. Finally, conclusion is drawn and future work are outlined in Sect. 6.

2 Mechanical Design and Composite Wave-driven Mechanics

2.1 Mechanical Design

2.1.1 Reinforcement of Undulating Fin and Bending Spring for Amphibious Case

In the early experiments, we use a 3 mm-thick membrane of silica gel to fabricate the undulating fin and install it on

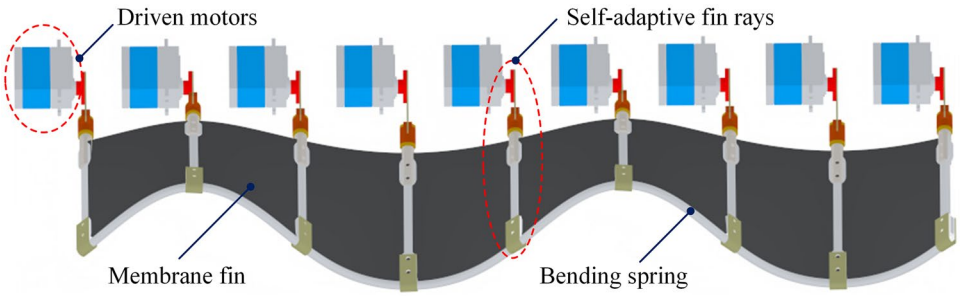

Fig. 1 The design of the novel amphibious undulating fin which has following distinguished features: (1) combination of flexible fin and bending spring, (2) self-adaptive fin rays, and (3) initial 3D undulating fin shape

the robot prototype. The result reveals that the sine wave can be only kept well when the robot is off the ground; and the wave is destroyed and transmits discontinuously when the robot is placed on the ground. We solved this problem by increasing the thickness of the membrane. However, the internal force is increasing rapidly and the actuation load becomes larger, although the stiffness is improved.

As the final scheme, a novel structure of undulating fin has been selected, which is strengthened by a long bending spring. As shown in Fig. 2, we fix the spring with the outer edge of the fin. By utilizing the elasticity of the thin flexible fin and the stiffness of long rigid spring, it can work well in the whole process of wave generating, wave keeping, and wave transmission. The undulatory propulsor is composed of several particular components, including: (1) membrane fin, (2) bending spring, (3) rubber tube, (4) fin rays, and (5) spring grippers. And the detailed explanation is as below.

(1) The membrane fin is composed of two complete sine waves, which guarantees that there are always two troughs touching the ground so as to keep stable, as shown in Fig. 2a.
(2) The bending spring is installed along the outer arc of the membrane fin and is clamped by nine spring grippers, as shown in Fig. 2b.
(3) The rubber tube is used to cover the bending spring and increase the friction with ground, as shown in Fig. 2c.
(4) Each fin ray is made of a pair of elastic steel slices, which have sufficient stiffness to transmit wave and also keep certain elasticity when touching the ground, as shown in Fig. 2d. The tail of the fin ray is connected with the spring gripper.
(5) The spring gripper is specially designed as two parts for assembling. The inner hole is designed with a T-shaped thread to match the gap of the bending spring, as shown in Fig. 2e, f. As a result, the spring can rotate but cannot transform in the inner hole, which avoids twisting the spring and prevents additional resistance.

2.1.2 Self-Adaptive Oscillating Fin Rays with Two Passive Rotational Degrees of Freedom

To improve efficiency and reduce energy consumption, a kind of self-adaptive oscillation unit with three degrees of rotational freedom has been proposed. The structure of the oscillation unit is shown in Fig. 3a. The end-ray chuck can rotate in the sliding bearings, which are inserted into the rotating socket and are positioned axially by the screw. As a result, the fin rays which are connected with the chuck are able to rotate passively so as to adapt to the change of tangent while moving up and down. This is an improvement to traditional design scheme, in which case the fin ray has only one-degree-of-freedom, i.e., it can only oscillate around the baseline of the fin. It is obviously that rigid fin rays are easy to destroy the sine wave and separate the whole fin surface into multiple segments, as shown in Fig. 3b. In addition, the bending spring in our novel amphibious undulating fin will generate extra twist torque if the spring gripper cannot keep parallel to the tangent of the wave. The improved situation is shown in Fig. 3c, where the fin ray is always parallel with the tangent line and the waveform is complete.

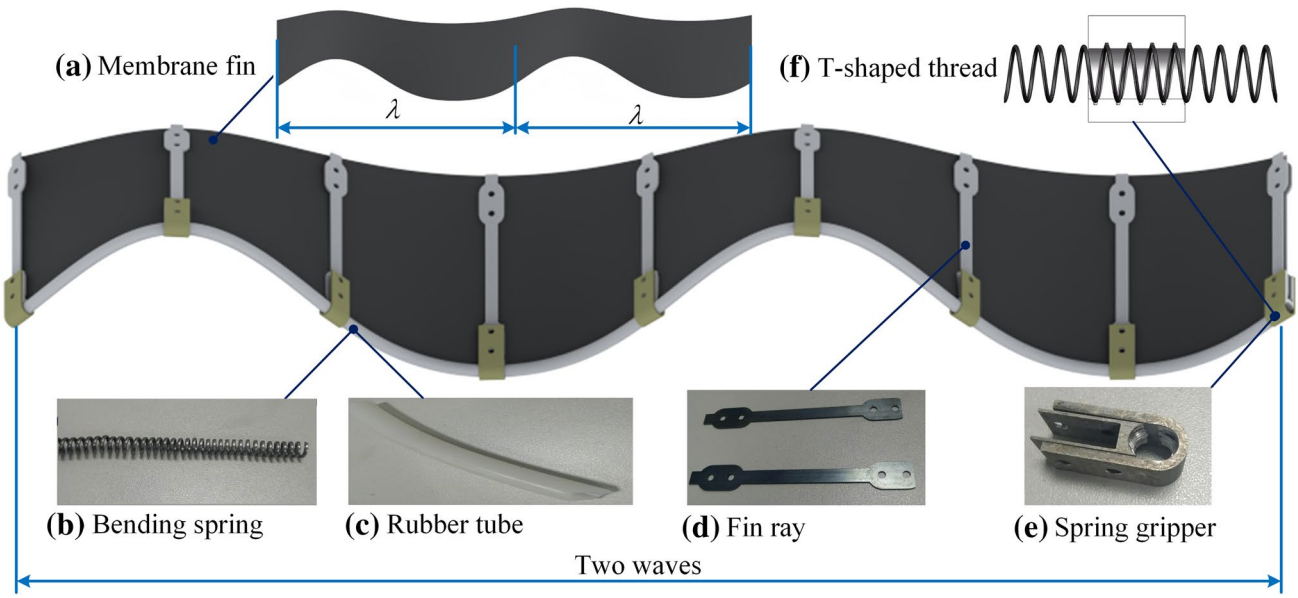

Fig. 2 The design of the novel amphibious undulating fin

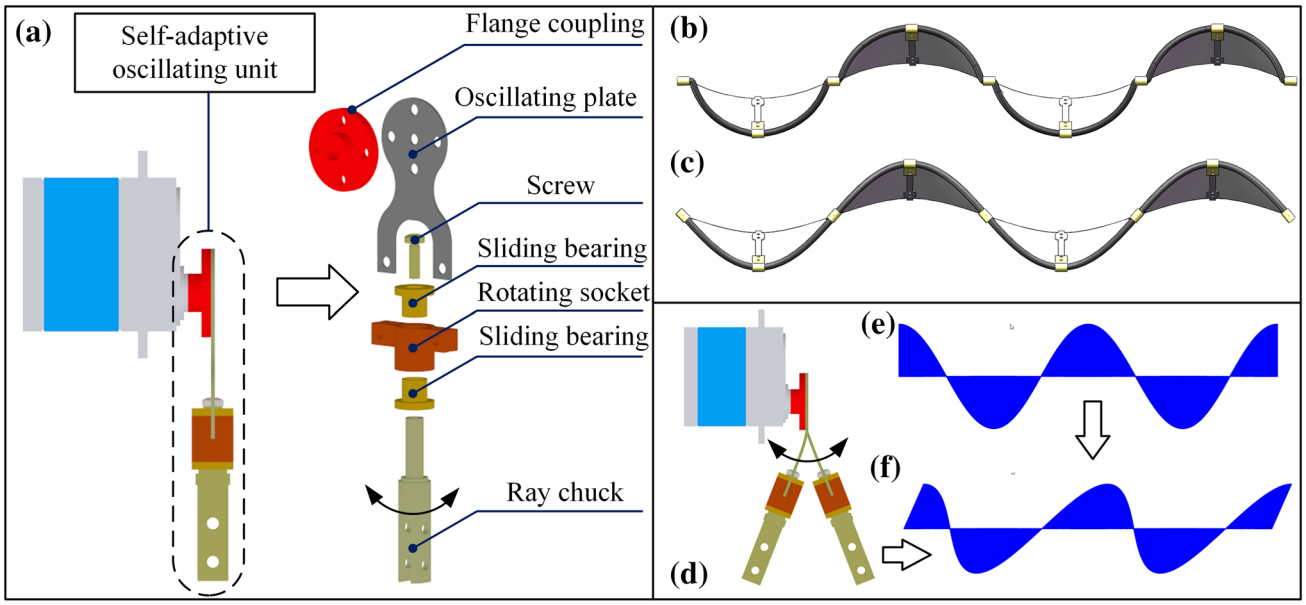

Fig. 3 The design of the self-adaptive oscillating unit. **a** The front view and the exploded view, **b** the undulating fin connected with fin rays that does not have rotational freedom; thus, the wave is separated into multiple pieces. **c** The improved undulating fin connected with self-adaptive fin rays, so the wave is complete. **d** The situation that the fin rays oscillate back and forth in the direction of wave propagation, thus generating a passive longitudinal wave. **e** The waveform of the undulating fin that has only transverse wave. **f** The waveform of undulating fin that has transverse wave and longitudinal wave

On the other hand, the oscillating plate is made of elastic steel and the thickness is as small as 0.6 mm, so it is easy to bend, which means that the whole self-adaptive oscillating unit has another degree of freedom, i.e., it can oscillate back and forth in the direction of wave propagation, as shown in Fig. 3d. As its oscillation direction is parallel to the robot body, we call it longitudinal wave, with respect to the actively generated transverse wave. Owing to the existence of the longitudinal wave, the waveform is no longer a standard sine wave, but a modulation wave, as shown in Fig. 3e, Fig. 3f. The interaction of the composite wave has significant and complex impact on the locomotion mechanism of the undulating fin, which will be analysed in detail in the following sections.

2.1.3 From 2D Arc-shaped Plane to 3D Sine Wave Fin

The present research involving undulating fin propulsor often uses a piece of membrane to form the fin surface. And all the fin rays are initialized to the same angle [32, 34, 36], as displayed in Fig. 4. This method is widely used because of the simple way to fabricate the membrane fin as well as the convenience of mechanical assembly. However, it is proved to be unsuitable for amphibious undulating fin propulsor. On the one hand, there will be large internal force generated by deformation of the planar fin, which will increase the load of servo motors. On the other hand, the undulating fin propulsor should always keep sine shape so as to support the robot body in land, which is not necessary in the conventional underwater case. To address these problems, we propose a new method to manufacture the undulating fin. As shown in Fig. 5, the 3D undulating fin is formed by straightening the 2D arc-shaped flexible sheet material and the sinusoidal shape is maintained by rigid fin rays. Suppose that the maximum oscillating angle is θ_m, the distance between internal/external arc of undulating fin and oscillating centre is R_1 and R_2. The sheet is stretched into sine-like waves, whose wavelength is λ and

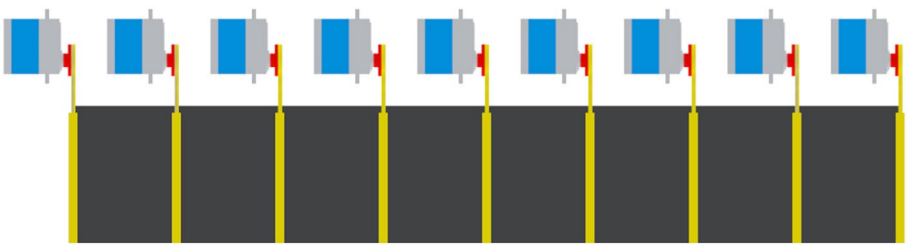

Fig. 4 Schematic diagram of conventional method of making undulating fin propulsor which is initialized as a planar sheet

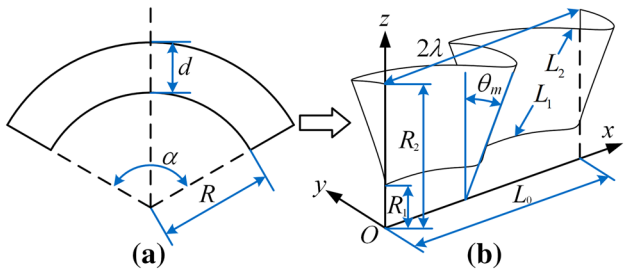

Fig. 5 The parameters of arc-shaped sheet and undulating fin

whole length is L_0. Here, we choose $L_0 = 2\lambda$. If we use x as the coordinate of Ox direction and r as the natural coordinate of fin direction, the initial surface can be expressed as Eq. (1)

$$\begin{cases} x(x,r) = x \\ y(x,r) = r\sin\left(\theta_{\mathrm{m}}\sin\left(\dfrac{2\pi x}{\lambda}\right)\right), \\ z(x,r) = r\cos\left(\theta_{\mathrm{m}}\sin\left(\dfrac{2\pi x}{\lambda}\right)\right). \end{cases} \begin{pmatrix} r \in [R_1, R_2] \\ x \in [0\ ,\ L_0] \end{pmatrix} \tag{1}$$

The shape of the original plane membrane fin can be fully described using the radius of inner edge (R), the width (d), and the fan angle (α). Owning to the constraints of boundary conditions, the length of inner edge (L_1), the outer edge (L_2), and the width (d) remain unchanged, as shown in Eq. (2)

$$\begin{cases} R\alpha = L_1 \\ (R+d)\alpha = L_2 \\ d = R_2 - R_1 \end{cases} \Rightarrow \begin{cases} R = (d\cdot L_1)/(L_2 - L_1) \\ \alpha = (L_2 - L_1)/(R_2 - R_1). \\ d = R_2 - R_1 \end{cases} \tag{2}$$

As our design parameters, R_1, R_2, λ, and θ_{m} determine the shape of undulating fin as well as the arc-shaped sheet. L_1 and L_2 can be calculated using curvilinear integration, as described in Eq. (3)

$$L_i = \int_{u=0}^{L_0} \sqrt{\left(\frac{\partial x}{\partial u}\right)^2 + \left(\frac{\partial y}{\partial u}\right)^2 + \left(\frac{\partial z}{\partial u}\right)^2}\,\mathrm{d}u, i = 1, 2. \tag{3}$$

The chosen parameters for the amphibious fin in this paper are shown in Table 1.

Table 1 The parameters of the undulating fin

λ/m	L_0/m	R_1/m	R_2/m	d/m	θ_{m}/°
0.4	0.8	0.05	0.155	0.15	25

2.2 Composite Wave Walking Mechanics

2.2.1 Simplified Equivalent Model of Undulating Fin

As has been mentioned above, the novel undulating fin generates two different waves with the oscillation of fin rays, including the transverse wave generated actively and the longitudinal wave generated passively. Since the mechanism of the longitudinal wave needs to be explored, it is difficult to describe the space equation of the undulating fin. To simplify the compound motion and conduct effective analysis, some assumptions are introduced and an equivalent model is established. As shown in Fig. 6a, when the oscillating amplitude is in a small scale, the space motion of the outer arc of the membrane fin, as well as the bending spring, is close to planar motion. The simplified model is depicted in Fig. 6b. Only one wave is analysed because of its periodicity.

The transformation rules for the simplified model are introduced below.

(1) The space motion of the fin surface is simplified to the plane motion of the bending spring.
(2) The oscillation of the fin ray is simplified as the up-and-down movement of the clamping point, as numbered in Fig. 6.
(3) The fin ray is simplified to a transverse spring attached to the clamping point which therefore can swing left and right under the constraints of spring, as shown in Fig. 6b.
(4) The clamping point is hinged to the bending spring and the transverse spring. And the hinges have no damping.

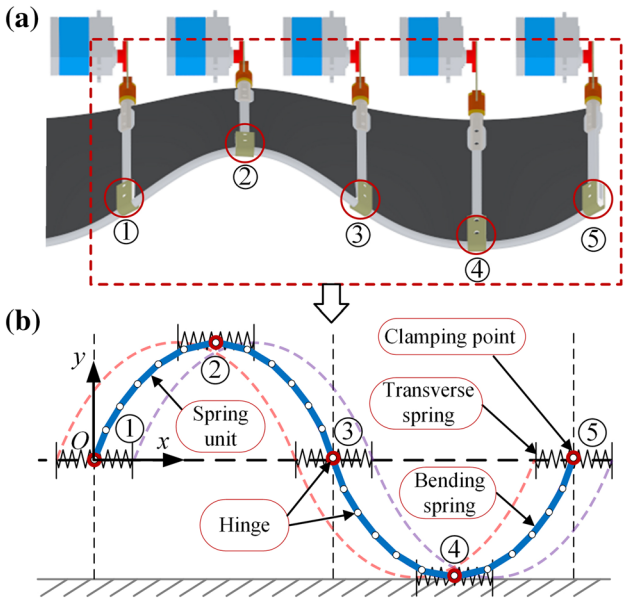

Fig. 6 The equivalent dynamic model of the composite wave

(5) The physical properties of the bending spring remain unchanged.
(6) Suppose the bending spring is composed of multiple micro-rigid units which are connected with hinges. The bending stiffness of the spring is equivalent to the torsional stiffness of hinges.

As optimal selection, the tensile stiffness of the bending spring is very large, so the stretch and compression of the bending spring can be ignored. We presume the length of the bending spring remains unchanged over time. In undulating process, the curvature of the bending spring (ρ_s) changes with time and position. If the bending stiffness is K_M, the bending moment (M) is proportional to the curvature ρ_s

$$M = K_M \cdot \rho_s. \tag{4}$$

The fin ray is equivalently replaced as the transverse spring. Due to the difference of tensile and shear stiffness, the bending spring tends to restore to straight state, which therefore generate a horizontal force (F_x) on the clamping point. As a result, the transverse spring will generate a displacement (Δx). This relationship is described by Hooke's law

$$F_x = K_P \cdot \Delta x. \tag{5}$$

2.2.2 Walking Mechanism of Composite Wave

Owing to the existence of the transverse spring and the bending spring, the outer arc of the undulating fin is no longer a standard sine wave when the wave propagates with time. The interaction of the clamping point and the transverse spring results in a longitudinal oscillation, which changes the wave from one dimension to two dimensions. This composite wave has a significant and complex impact on walking mechanism of the undulating fin. Based on the discrete element model in Sect. 2.2.1, the dynamic and kinematic analysis of the composite wave-driven mechanics can be conducted. For theoretical analysis, suppose that the adhesion between the ground and the robot is large enough and there is no slip between the ground and the clamping point or the bending spring.

As shown in Fig. 7a, the length of each spring segment between neighbouring clamping points is constrained. The initial length is calculated in Eq. (6), where A is the amplitude of the plane sine wave

$$C_0 = \int_0^{\frac{\lambda}{4}} \sqrt{1 + \left(\frac{\partial}{\partial x} A \sin\left(\frac{2\pi}{\lambda} x\right)\right)^2}\, \mathrm{d}x. \tag{6}$$

When the wave propagates at x-direction, the vertical coordinate of every clamping point is determined by the corresponding fin ray equation

$$y(i) = A \sin\left[\delta \cdot 2\pi f t + (i-1)\pi/2\right] = A \sin\left[\Phi_i\right],\ i = 1-5. \tag{7}$$

In Eq. (7), f is the undulating frequency, $\delta = \pm 1$ means negative or positive wave direction, and Φ is the angle phase.

The vertical velocity of clamping point is

$$v_{iy} = y'(i) = 2\pi f A \delta \cos\left(\delta \cdot 2\pi f t + (i-1)\varphi\right),\ i = 1-5. \tag{8}$$

When the wave propagates, the ideal length of each spring segment changes at difference phase

$$C_i = \int_{\frac{\lambda}{2\pi}\Phi_i}^{\frac{\lambda}{2\pi}\left(\Phi_i + \frac{\pi}{2}\right)} \sqrt{1 + \left(\frac{\partial}{\partial x} A \sin\left(\frac{2\pi}{\lambda} x\right)\right)^2}\, \mathrm{d}x,\ i = 1-4. \tag{9}$$

Equation (8) shows that the velocity of a clamping point is fastest at equilibrium position and slowest near peaks and valleys. Since all clamping points are at different phase, there are relative velocity and force between adjacent points, as depicted

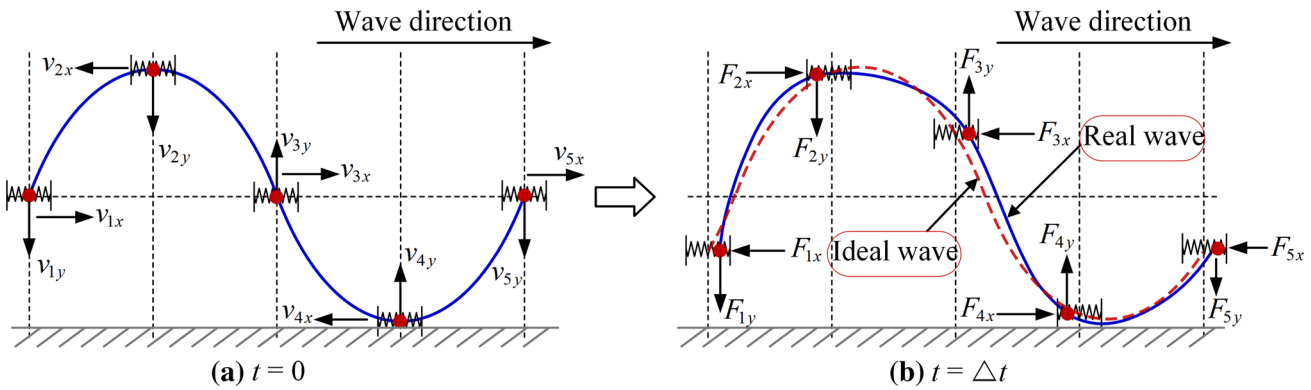

Fig. 7 Kinematic and dynamic analysis of the simplified model for the undulating fin

in Fig. 7a. As a result, the wave is no longer a standard sine shape, as shown in Fig. 7b.

This contradiction of ideal length and real length of bending spring can also be calculated by Eq. (9). When $t=\Delta t$, $C_1>C_0$, $C_2<C_0$, $C_3>C_0$, $C_4<C_0$, the neighbouring clamping points should move either closer or further in horizontal direction. The relative motion of all clamping points is showed in Fig. 7b. The y-force given by servo motors is the same with y-velocity; and the x-force generated by transverse spring is opposite with the relative x-displacement.

Based on these kinematic and dynamic analysis, we can divide the whole motion into two kinds of situations. (a) $t\neq kT/4\pm\Delta t$. The clamping points are all hanging on the ground and only the bending spring is touching the ground. (b) $t=kT/4\pm\Delta t$. The clamping points is moving nearing the ground.

(a) Walking mechanics when the spring touches ground

First, the generous situation (a) is considered. We treat the spring segments as discrete elements, as shown in Fig. 8. As a whole segment, the x-force F_{ix} and F_{jx} generated by transverse spring at two ends can be regard as a pair of actions and they are be ignored. The driven force F_{i0} and F_{j0} is provided by the fin rays, which are actuated by servo motors. The spring unit can be considered as a two-force bar. The force between the units can be calculated by static balancing condition, as Eq. (10), where $\alpha_{k,k-1}$ and $\beta_{k,k-1}$ are the angle of neighbouring units in left and right side. M and N are the unit number in left and right sides, respectively

$$\begin{aligned} F_{ik} &= F_{i\cdot k-1}\cdot\cos\left(\alpha_{k,k-1}\right),\ k=1,2,\ldots M \\ F_{jk} &= F_{j\cdot k-1}\cdot\cos\left(\beta_{k,k-1}\right),\ k=1,2,\ldots N. \end{aligned} \tag{10}$$

The maximum driven force is determined by the power of servo motors. If the maximum torque is T_{m}, the maximum action force on the ground can be calculated by Eq. (11). Under the assumption of no slippage, the ground friction is equal to the actuation force, as described in Eq. (12)

$$F_{\max}=\frac{T_{\mathrm{m}}}{R}\left(\prod_{k=1}^{M}\cos\left(\alpha_{k,k-1}\right)+\prod_{k=1}^{N}\cos\left(\beta_{k,k-1}\right)\right) \tag{11}$$

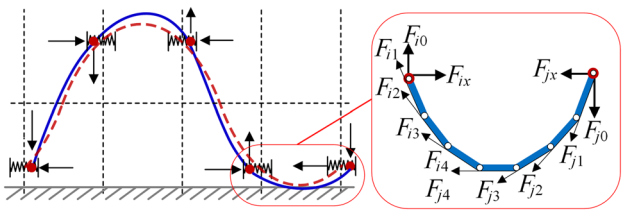

Fig. 8 The discrete element analysis when the bending spring touches the ground

$$f_{\max}=F_{\max}. \tag{12}$$

(b) Walking mechanics when the clamping points touch ground

For situation (b), the spring segments between neighbouring clamping points can be treated as a whole. Taking the analysis method in Fig. 7, a complete analysis is conducted in one period of wave propagation. The shape of the wave and the relative position of all clamping points are shown in Fig. 9. From the whole locomotion process, the following laws of motion can be obtained:

(1) All the clamping points contact the ground in a fixed turn. They all move forward relative to the body before contacting the ground and then move back in the following interaction process with the ground. This shows that the clamping points make reciprocating motion about the equilibrium position in horizontal direction.
(2) In a period of motion, the horizontal velocity direction of every clamping point changes periodically, which is similar to a longitudinal wave generated passively.
(3) The effect of relative motion between the clamping point and the robot body tend to increase the forward velocity. If the velocity of undulating fin is v_{f} and the velocity of clamping point is Δv_{p}, the robot velocity is $v=v_{\mathrm{f}}+\Delta v_{\mathrm{p}}$.

In summary, the robot gains actuation force from the ground during the whole undulating period. The passive longitudinal wave will produce a velocity additive effect, which is similar to wheel kinematics. As a result, the composite wave will improve walking velocity.

2.3 Swimming Mechanics

The robot gains propulsion force from the bilateral fins which squeeze surrounding fluid and change the flow field pressure distribution during the undulating motion underwater. There are several theories for calculating the thrust force of moving objects in flow fluid, including actuating disc theory, reaction force theory, fluid resistance theory, and fluid drag theory. To get a theoretical understanding of the propulsion force, we use the fluid drag theory to build the dynamic model of the undulating fin. As a simplified quasi-steady method, the fluid drag theory has been widely used for underwater objects and has been proved to be effective.

As shown in Fig. 10, the undulating fin is meshed into multiple micro-face elements. Based on the assumption of fluid drag theory, the force on any face element is consisting of resistance and viscous force. The resistance is the normal stress applied by the fluid to the face element, and the viscous force is the shear stress applied by the fluid to the face element. They can be calculated as Eq. (13)

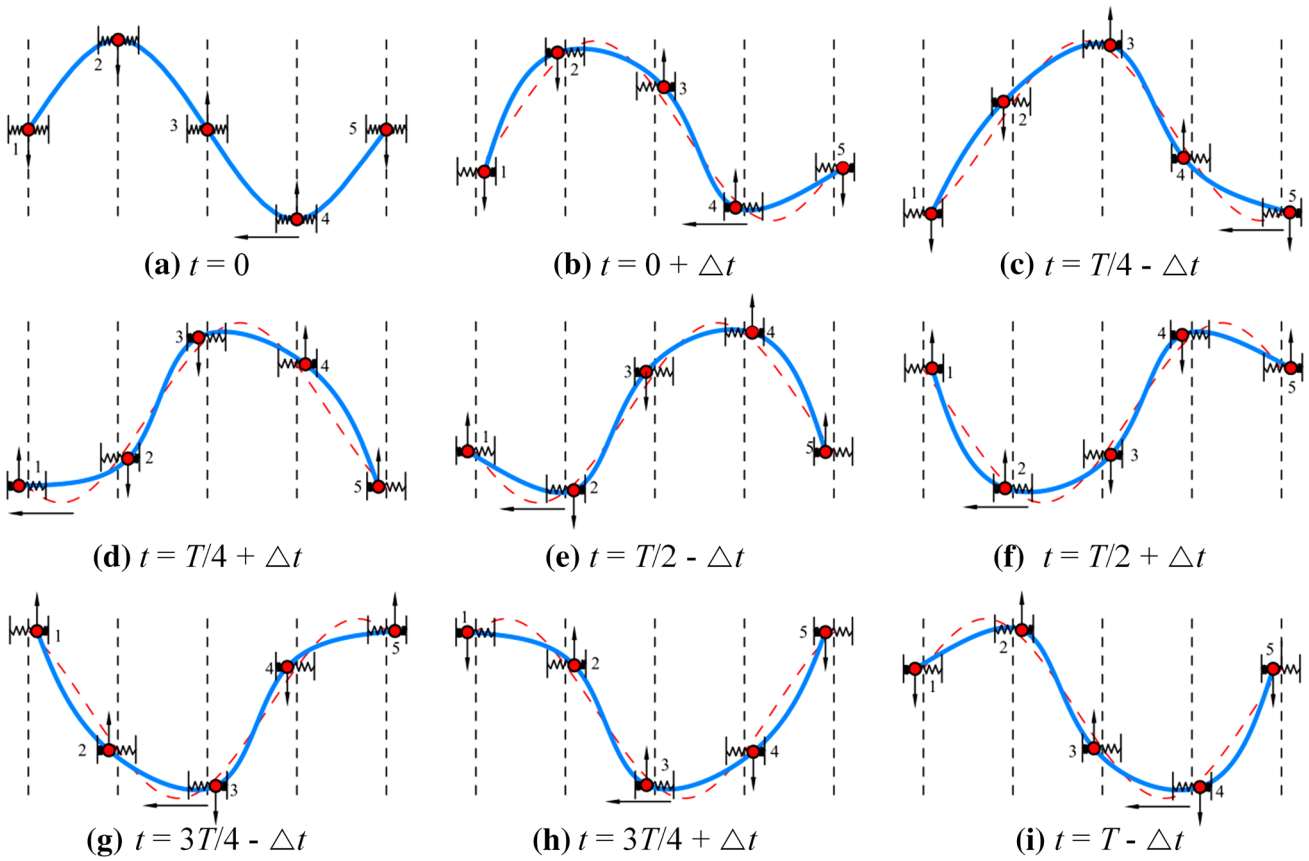

Fig. 9 The steps of walking process of undulating fin in a period of motion

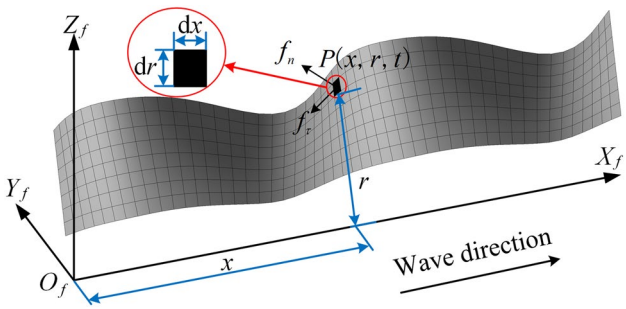

Fig. 10 The dynamic model of the undulating fin

$$\begin{cases} \vec{f}_n = \vec{F}_n / \mathrm{d}S = -\frac{1}{2}\rho C_s \left\| \vec{v}_n \right\|^2 \vec{v}_{n0} \\ \vec{f}_\tau = \vec{F}_\tau / \mathrm{d}S = -\frac{1}{2}\rho C_\tau \left\| \vec{v}_\tau \right\|^2 \vec{v}_{\tau 0} \end{cases}, \tag{13}$$

$\vec{v}_n$ and $\vec{v}_\tau$ are the normal and tangential velocity of the face element, respectively. $\vec{v}_{n0}$ and $\vec{v}_{\tau 0}$ are their unit vectors. ρ, $\mathrm{d}S$, C_s, and C_τ are the fluid density, the face element area, the resistance coefficient, and viscous force coefficient, respectively.

Suppose the wave direction is represented by δ, which can be 1 or -1 as forward and back propagation. When the undulating fin is f, the motion equation of the fin is

$$\theta(x,t) = \theta_m \cdot sin\left(\delta \cdot 2\pi f t + \frac{2\pi}{\lambda} x\right). \tag{14}$$

The position of face element P can be calculated in three-axis components in fin coordinate system

$$\begin{cases} {}^f P_x(x,r,t) = x \\ {}^f P_y(x,r,t) = r \cdot \sin\left[\theta_m \cdot sin(\delta \cdot 2\pi f t + 2\pi x/\lambda)\right] \\ {}^f P_z(x,r,t) = r \cdot \cos\left[\theta_m \cdot sin(\delta \cdot 2\pi f t + 2\pi x/\lambda)\right]. \end{cases} \tag{15}$$

And the velocity of face element P can be obtained in fin coordinate system, as shown in Eq. (16)

$${}^f\vec{V}_p = \left[\frac{\partial P_x(x,r,t)}{\partial t}, \frac{\partial P_y(x,r,t)}{\partial t}, \frac{\partial P_z(x,r,t)}{\partial t}\right]^T. \tag{16}$$

When the robot moves at OX_e direction, the velocity of the robot in inertial coordinate system is

$$^{e}\vec{V}_c = \left(U_x, 0, 0\right)^{\mathrm{T}},\ ^{e}\vec{\omega}_c = (0,0,0)^{\mathrm{T}}. \tag{17}$$

The absolute velocity of the element P in inertial coordinate system is

$$^{e}\vec{V}_p = {}^{f}\vec{V}_p + {}^{e}\vec{V}_c = \left(U_x, r\cos\theta\cdot\theta_t', -r\sin\theta\cdot\theta_t'\right)^{T}. \tag{18}$$

The normal vector of P is calculated by its gradient and the unit vector can be obtained

$$\vec{n} = \frac{\partial\vec{P}(x,r,t)}{\partial x}\times\frac{\partial\vec{P}(x,r,t)}{\partial r} = \left(r\theta_x', -\cos\theta, \sin\theta\right)^{\mathrm{T}} \tag{19}$$

$$\vec{n}_0 = \frac{\vec{n}}{\|\vec{n}\|} = \frac{1}{\sqrt{1+\left(r\theta_x'\right)^2}}\left(r\theta_x', -\cos\theta, \sin\theta\right)^{\mathrm{T}}. \tag{20}$$

We can get the normal velocity and shear velocity of the face element P relative to the static fluid

$$\vec{v}_n = \left(^{e}\vec{V}_p\cdot\vec{n}_0\right)\cdot\vec{n}_0 = \frac{r\left(-\theta_t'+\theta_x'U_x\right)}{1+\left(r\theta_x'\right)^2}\left(r\theta_x', -\cos\theta, \sin\theta\right)^{\mathrm{T}}. \tag{21}$$

The unit vector of $\vec{v}_n$ is

$$\vec{v}_{n0} = \frac{sign\left(-\theta_t'+\theta_x'U_x\right)}{\sqrt{1+\left(r\theta_x'\right)^2}}\left(r\theta_x', -\cos\theta, \sin\theta\right)^{\mathrm{T}}. \tag{22}$$

Taking the chord length of undulating fin as the dimensionless characteristic length and the lateral velocity of upper edge of undulating fin as the characteristic velocity, The Lehmann number Re is

$$Re = \frac{V\lambda}{v} = \frac{\theta_m\cdot 2\pi f d\lambda}{v} = 1.63\times 10^5. \tag{23}$$

Since the value Re is in higher range, the effect of viscous force can be ignored. The fluid force acting on the flexible fin during the undulating motion is

$$\vec{F} = \vec{F}_n + \vec{F}_\tau = \vec{F}_n = -\frac{1}{2}\rho\int_{R_1}^{R_2}\int_{0}^{L_0} C_{\mathrm{s}}\frac{r^2\left|\theta_t'-\theta_x'U_x\right|^2}{1+\left(r\theta_x'\right)^2}\cdot\frac{\mathrm{sign}\left(-\theta_t'+\theta_x'U_x\right)}{\sqrt{1+\left(r\theta_x'\right)^2}}\begin{pmatrix} r\theta_x' \\ -\cos\theta \\ \sin\theta\end{pmatrix}\mathrm{d}x\mathrm{d}r. \tag{24}$$

The pressure coefficient C_s is related to the shape of the undulating fin, which cannot be directly derived and needs to be identified by simulation and experiment. We set $C_s=1$ for the qualitative trend of dynamic force. Suppose the baseline of the undulating fin is fixed, i.e., $U_x=0$. Setting the frequency is $f=2$ Hz, the direction is $\delta=1$ and $L_0=2\lambda$, and the three-axis force of a single fin is calculated using numerical integration. As shown in Fig. 11a, the forces at three axes are called thrust force, lateral force, and lift force, respectively. As the comparison, we keep f and L_0 and change the wave number as incomplete value, which is $L_0=2.25\lambda_1$. The result is shown in Fig. 11b. More wave numbers are calculated later and the result is shown in Fig. 11c, in which the mean forces and their standard deviations are marked with vertical bar. Furthermore, the mean thrust force is calculated at different frequency, as shown in Fig. 11d. From the calculation results, the following conclusions are drawn.

(1) The undulating fin mainly generates thrust force, which changes periodically and the frequency is the twice of the undulating frequency. Both the lateral force and lift force change periodically and the mean values are zero.
(2) When the waveform is composed of two waves, the variation range of thrust force is relatively small. Besides, the amplitude of lateral force and lift force is small. However, the variation amplitudes of all the three-axis forces increase rapidly when the wave number is 2.25, especially for the lateral force.
(3) The standard deviation of both thrust force and lift force are small when the wave number is a multiple of 0.5. And the deviation of lateral force is approximately zero only when the wave number is integer. Therefore, complete wave is beneficial for both decreasing thrust fluctuation and eliminating lateral and lift forces.
(4) The thrust force and frequency are approximately in a second-order relationship.
(5) The propulsion force and velocity are opposite on land and water environment. In other words, the propulsion force and velocity are the same with wave direction for land walking, while they are the opposite with wave direction for underwater propulsion.

3 Simulation for Land Walking

3.1 The Virtual Prototype

3.1.1 Implementation of the Simulation Model

To verify the dynamic analysis result, a virtual prototype based on discrete element model is established to simulate the locomotion process. From the visual simulation and data monitoring, the specific kinematic and dynamic mechanism would be clearly demonstrated.

The simulation model is shown in Fig. 12. The bending spring is segmented into multiple small units, which contains two cases. The first type which are shown in orange are the middle parts that do not connect with clamping

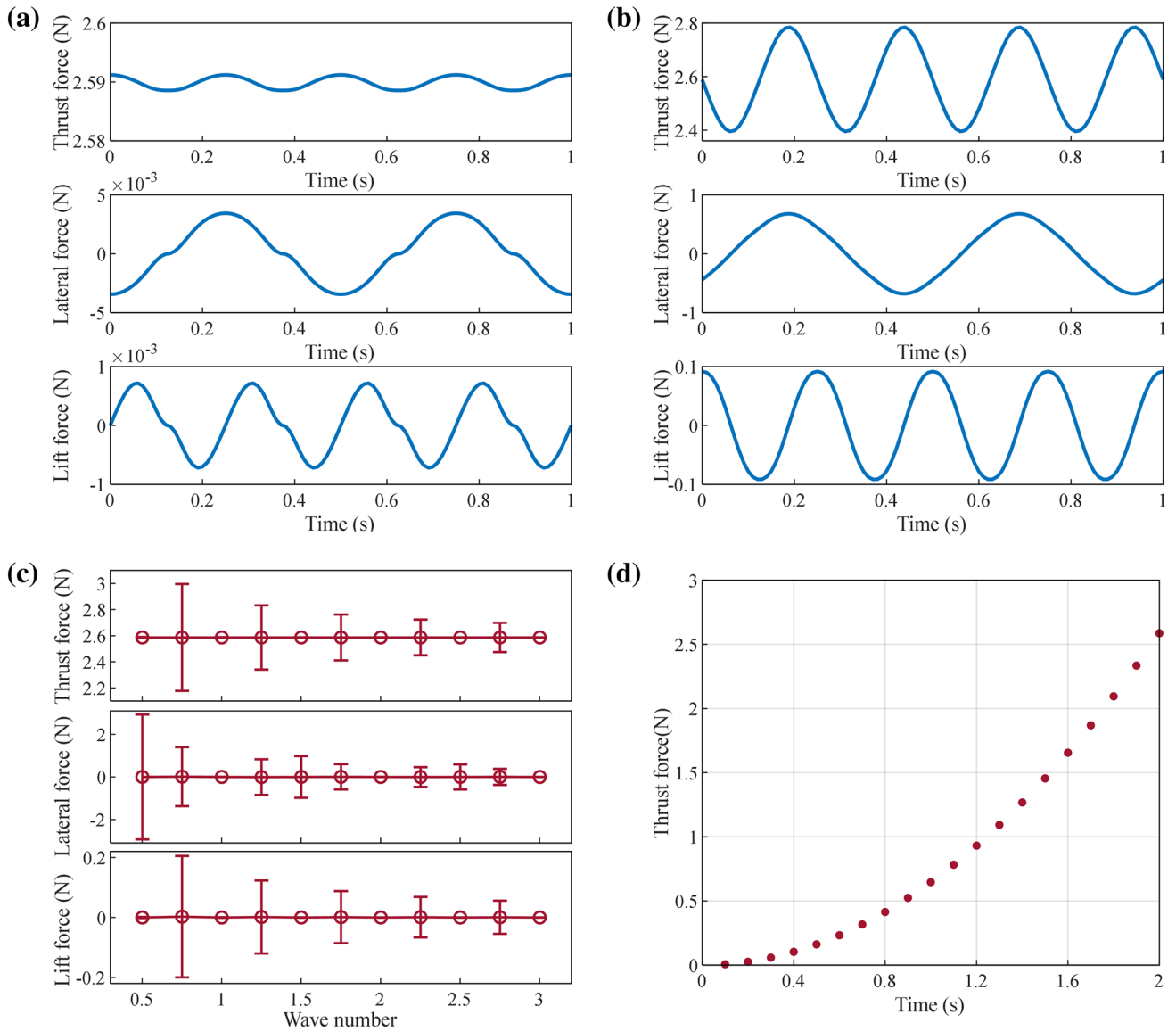

Fig. 11 The numerical calculated force. **a** $f=2$ Hz, $L_0=2$ waves. **b** $f=2$ Hz, $L_0=2.25$ waves. **c** The forces at different wave number with vertical bars to show the standard deviation. **d** The mean thrust force at different frequency

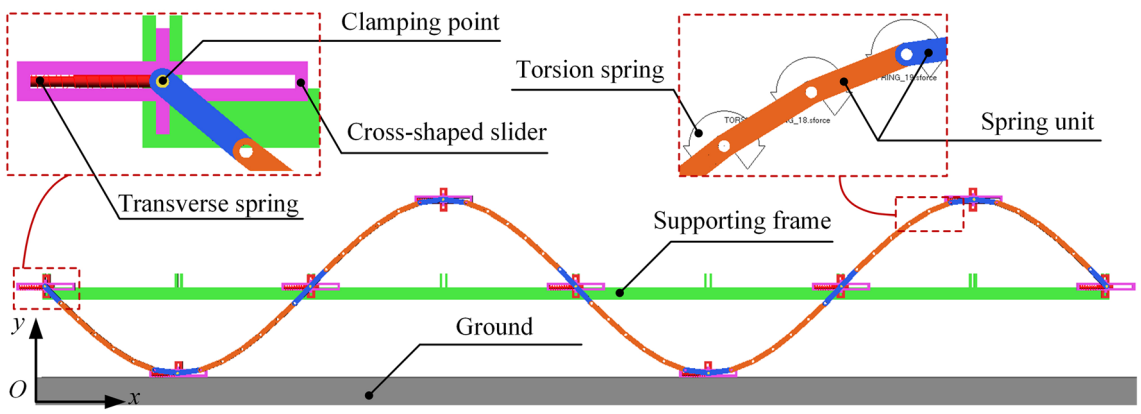

Fig. 12 The simulation model of undulating fin for walking mechanism in ADAMS software

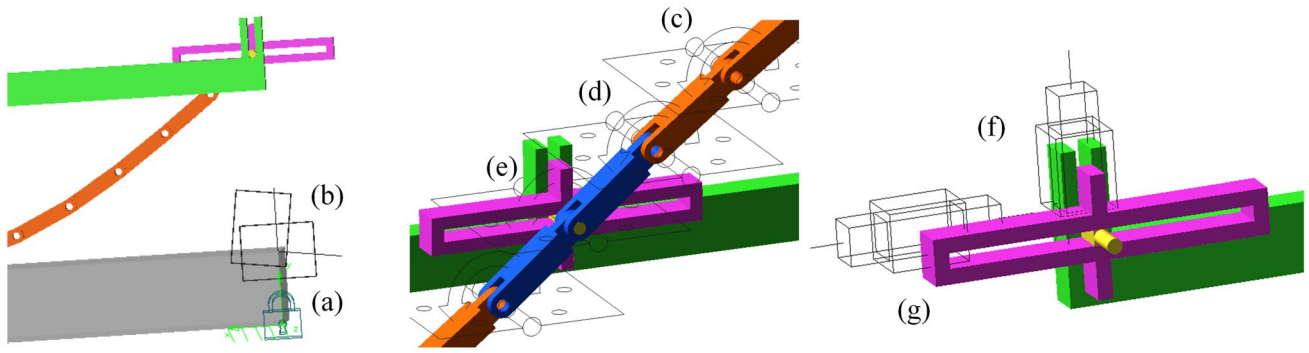

Fig. 13 The constraints and boundary conditions of the virtual prototype in ADAMS software

points, and the second type shown in blue are the parts connected with clamping points. The spring units are connected with each other by hinges, and the second group of units are also hinged to the clamping points. Apart from the bending spring, all other parts of robot are treated as a rigid body. The clamping point is designed as a brick-shaped body whose tail section is cylindrical so as to hinge with spring units. Here, a special cross-shaped slider is designed to simulate the active up-and-down motion and the passive left-and-right motion of the clamping point. A long support frame, with vertical groove at equal distance, is used to represent the robot body. And a rectangular plate is used to represent the ground.

3.1.2 Constraints and Boundary Conditions

All the components interact with each other by various constraints and boundary conditions. First, the grey rectangular plate is connected to ground by fixed joint, so it can be regarded as the ground, as shown in Fig. 13a. Then, a planar joint is applied to the supporting frame and the ground, guaranteeing that the robot prototype can only move in the horizontal *xz*-plane and cannot tilt around the *x*-axis of the body, as shown in Fig. 13b. This restriction is reasonable, because our real robot is supported by two undulating fins and the body is in balance. Second, the spring units are connected with each other by revolute joint so as to simulate the flexible spring, and revolute joints are also applied between spring units and clamping points for power transmission, as shown in Fig. 13c–e. Third, two prismatic joints are set around the cross-shaped slider. The prismatic joint between the slider and the supporting frame (Fig. 13f) restricts that the slider can only move up and down in the groove of the supporting frame. And the joint between the slider and the clamping point (Fig. 13g) enables the clamping point to move horizontally.

Various forces are applicated to the system so as to simulate the dynamic behaviour. As shown in Fig. 12, we use a compression–tension spring damper in ADAMS software to represent the transverse spring and a torsion spring damper to represent the bending spring. The compression–tension spring damper should be set inside every nine sliders and the torsion spring damper is set in each revolute joint between the spring units. Finally, all the discrete spring units are kept friction contact constraint with the ground.

Table 2 Parameters of the virtual prototype model

Parameter type	Physical fin	Virtual prototype
Wavelength λ (mm)	400	400
Amplitude θ_m (°)	25	–
Maximum radius R_2 (mm)	155	–
Wave amplitude A (mm)	–	63.39
Phase difference φ(°)	90	90
Wave number	2	2
External arc length (mm)	981.44	981.52
Number of spring units	–	56
Length of spring units (mm)	–	17.52

Table 3 Parameters of the springs

Spring type	Stiffness	Damping
Torsion spring	5 N/degree	0.01
Transverse spring	0.2 N/mm	0.01

3.2 Simulation Result

Table 2 gives the parameters of the designed undulating fin and the simplified virtual prototype model. The stiffness coefficient and damping coefficient of transverse spring and torsion spring are then set according to the selected elastic steel slice and the bending spring, as shown in Table 3.

To simulate the real motion of the composite wave of the undulating fin, we set the cross-shaped slider as the driving part instead of the clamping point. And the motion is applied at the prismatic joints between the slider and

the supporting frame. If starting at equilibrium position, the motion function of ith slider can be described below

$$y(i) = A\sin\left[2\pi ft + (i-1)\frac{\pi}{2}\right],\ i = 1, 2, \ldots 9. \tag{25}$$

Owning to face contacts, the clamping points oscillate vertically in a fixed phase difference just as well as the sliders. And the clamping point oscillate horizontally inside the slider with the deformation of the bending spring. Simulation is conducted to evaluate the composite wave and its effect on walking propulsion. Setting the simulation time as 3.0 s and the time step as 0.01 s, the simulation animation has been obtained and the video sequence is shown in Fig. 14. The simulation results show that the virtual prototype successfully realizes the land walking function and exhibits good motion form in the whole process. With the transverse wave propagates forward, the curve of the bending spring simulated by discrete units maintains well and the robot body moves forward relative to the ground. The black dotted line in Fig. 14 presents the position of the centre of the supporting frame, which shows that the prototype walks along at a relatively constant speed.

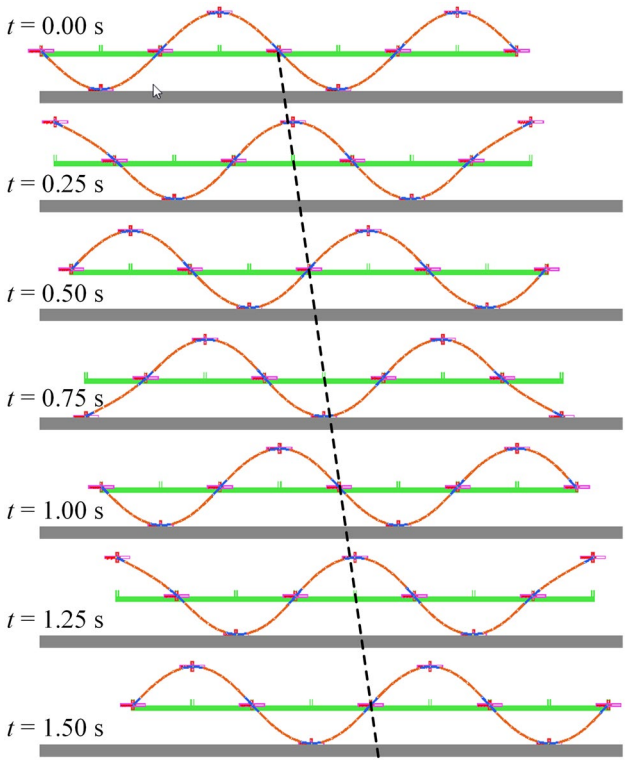

Fig. 14 The simulated motion of the discrete element model at 1 Hz frequency in ADAMS software

3.3 Discussion

To accurately evaluate the motion law of the prototype in the simulation process, the horizontal velocity and displacement of the mass centre have been recorded in Fig. 15. It can be noted that the displacement curve is relatively flat and the prototype has moved about 305 mm. In comparison, the velocity curve fluctuates around the average value, which is about 100 mm/s. And there are 4 peaks and 5 valleys in one period. Figure 16 presents the trajectory of the mass centre in xy-plane, which reveals that the supporting frame ups and downs at a fixed frequency when moving forward, which is about 1 Hz, as same as the undulating frequency of clamping points.

To get a clearer picture of the relationship between velocity and states of motion, a velocity–phase curve has been drawn in Fig. 17. The velocity peaks and troughs have been

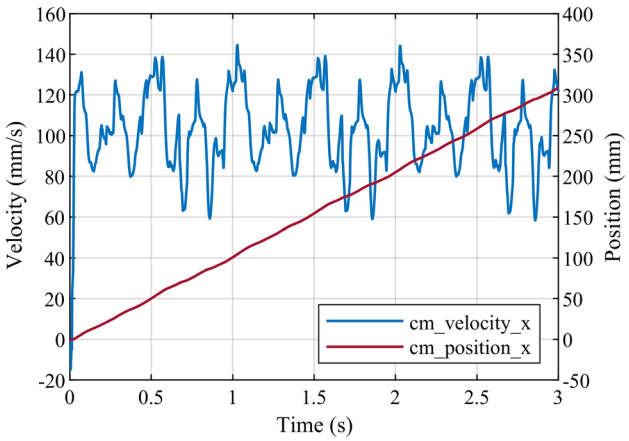

Fig. 15 The horizontal velocity and position of the simulation model's centre of gravity

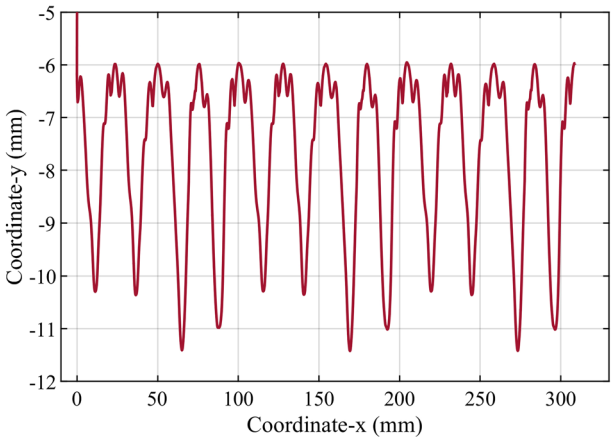

Fig. 16 The trajectory of the mass centre of the simulation prototype in xy-plane

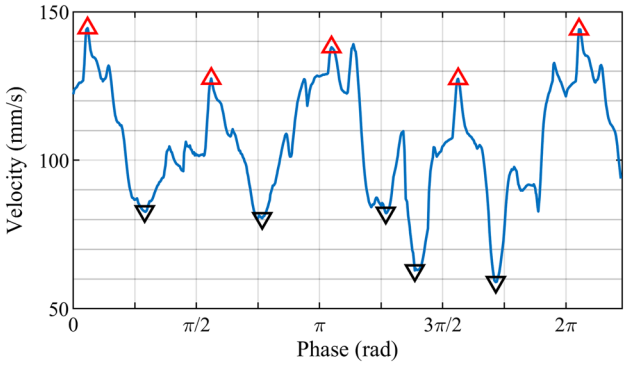

Fig. 17 The velocity–phase curve of the simulation prototype. The peaks are marked by red upper triangle and the troughs are marked by black lower triangle

marked in red upper triangle and black lower triangle, which illustrates that the peak appears near the phase in (0, $\pi/2$, π, $3\pi/2$, 2π), and the valleys near ($\pi/4$, $3\pi/4$, $5\pi/4$, $7\pi/4$). This is to say, when the clamping points touch the ground, there tend to be a larger speed and the robot reaches the peak speed at a short delay. The reason why there is several peaks in one period is that the clamping points contact the ground according to the phase sequence.

According to the dynamic analysis in Sect. 2, the space motion of the clamping point leads to a composite wave, i.e., the transverse wave and longitudinal wave, respectively. Figure 18 gives the horizontal movements of all the clamping points relative to the supporting frame. The following rules can be obtained.

(1) All the points oscillate left and right near the equilibrium position. And the motion curve is approximately a sine wave, verifying that the clamping points have generated longitudinal wave passively when propagating transverse wave.
(2) The motion of adjacent clamping points is exactly opposite. In other words, their phase difference is 180°. The result is that point 1, 3, 5, 7, and 9 have the same phase, and the point 2, 4, 6, and 8 have an opposite phase.
(3) The frequency of the longitudinal wave is 2 Hz, which is twice of the transverse wave.
(4) The clamping points 1 and 9 are at the free end, and their relative motion curves are neither symmetrical nor regular, which is different from the medium points.

To more clearly present the motion of the clamping point relative to the supporting frame, the relative motion trajectory curve has been drawn in Fig. 19. It is obvious that the shape of the trajectory is similar to figure-of-eight, which also proves the frequency doubling effect between the two kinds of waves. The trajectory also proves the dynamic analysis in Sect. 2. It shows that the clamping points are always moving back relative to the robot body either near peaks or near valleys. If the fin crawls in a cave, both the upper face and the lower face of the ground will generate propulsion forces.

4 Experimental Verification of the Amphibious Robot Prototype

4.1 Implementation of the Robot Prototype

To verify the simulation results and observe the locomotion performance of the biomimetic undulating fin, a robot prototype which is equipped with a pair of the novel undulating

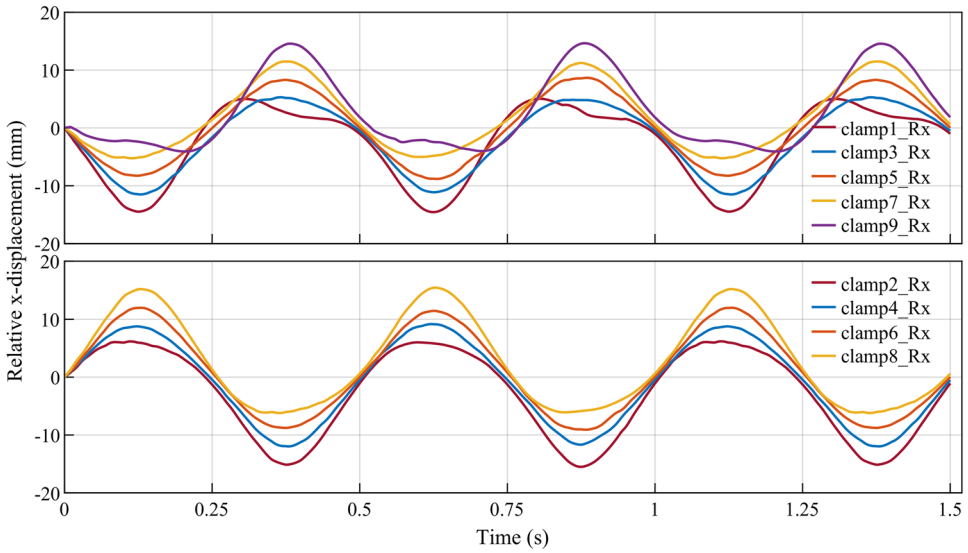

Fig. 18 The trajectory of the clamping point relative to the supporting frame

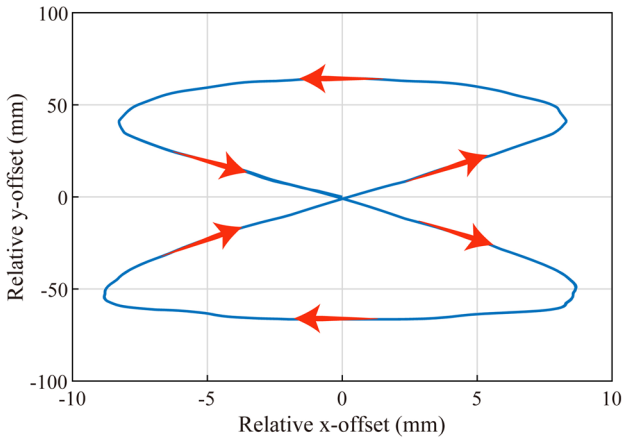

Fig. 19 The absolute trajectory of the clamping point relative to the supporting frame

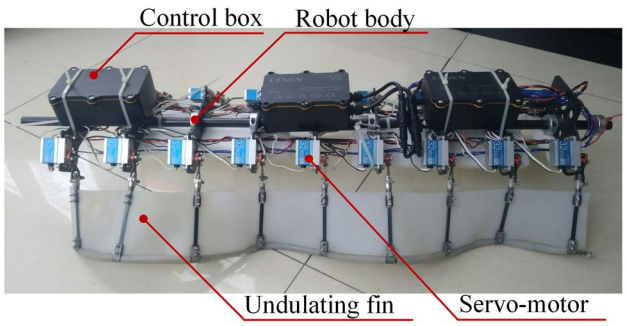

Fig. 20 The robot prototype

Fig. 21 The novel undulating fin unit

Table 4 Parameters of the robot prototype

Parameters	Value
Length (mm)	850
Width (mm)	224–534
Height (mm)	126–266
Weight on land	4.75
Weight underwater	4.75–6.75
Weight of a single fin	0.97
Fin material	Silica gel

Fig. 22 State of different deflecting angle of the robot

fins has been developed. As shown in Fig. 20, the prototype is composed of the robot body, the undulating fin unit, servo motors, and electronic boxes. The robot body is a combination of modular parts made by carbon plate and carbon tube. The undulating fin unit, which is shown in Fig. 21, is fabricated according to the design parameters in Sect. 2. A waterproof servo motor with torque of 32 kg has been selected to simplify the sealing structure and reduce the weight. The watertight control boxes are used to contain the control circuit boards, lithium batteries, and communication receivers. Besides, the control boxes also work as adding counterweight blocks so as to change the robot weight underwater. The parameters of the robot are shown in Table 4.

A 32-bit chip (STM32F767IGT6, 216 MHz) is used as the microcontroller of the main control board, which receives command from the remote controller (2.4 GHz) via a wireless receiver. The remote signals are then processed to generate the control parameters such as undulating frequency, direction, and equilibrium position. The real-time rotation angles of all servo motors are then calculated according to the undulating differential equations and converted into PWM signals. Finally, the second control board receives the PWM signals via serial port communication and drives the motors to move to the corresponding angle. Motion pictures are captured and saved by a high-speed camera (GoPro) in the experiments.

4.2 Land Experiment

The oscillating frequency and the deflecting angle have been considered as the main factor which affect the walking speed. As shown in Fig. 22, the deflecting angle, referring to the offset between the equilibrium position and the robot body, can be changed in the range of 0°–90°. First, the electromechanical and control system was verified and the manoeuvrability of the robot prototype was tested. Figure 23 gives the linear motion pictures of the robot when we set the frequency of both left and right undulating fin as 1.6 Hz and the deflecting angle as 45°. The robot moved straight at about 80 mm/s. Figure 24 shows the steering motion pictures when the undulating frequency of two sides were different (the left is 1.6 Hz and the right is 0.5 Hz).

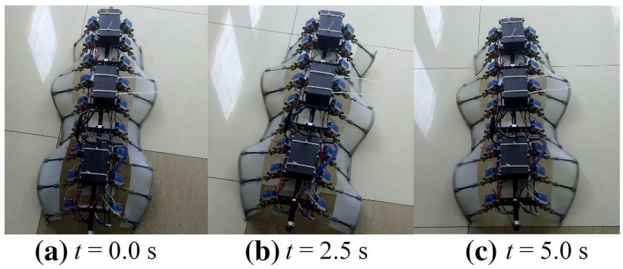

Fig. 23 Linear motion pictures of the robot

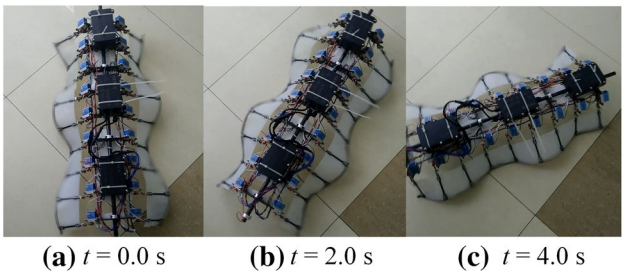

Fig. 24 Steering motion pictures of the robot

To evaluate the effect of oscillating frequency and deflecting angle on walking velocity, A serial of comparative experiments have been conducted. In those experiments, the linear motion was focused on, so the undulating frequencies of the two fins were set the same. A set of frequency ranging from 0.4 to 2 Hz and a set of deflecting angles ranging from 15° to 90° were selected to control the robot prototype. Figure 25 presents the velocity at different frequency and deflecting angle. The following conclusion can be obtained:

(1) Keeping the frequency unchanged, the velocity at different deflecting angle differs slight when the angle is large. However, the velocity declined rapidly when the deflecting angle is small than 30 degrees.
(2) Keeping the deflecting angle as the same, the walking speed increases with the increase of frequency.
(3) When the deflecting angle was zero, the robot prototype could not move forward and just moved to transverse side.

The locomotion experiments reflect that the relationship between walking speed and frequency is approximately linear. At the same time, the deflecting angle has little influence on the walking speed within a certain range. To reduce the length of the moment arm and the resistance consumption, the deflecting angle can be selected as small as possible in practice.

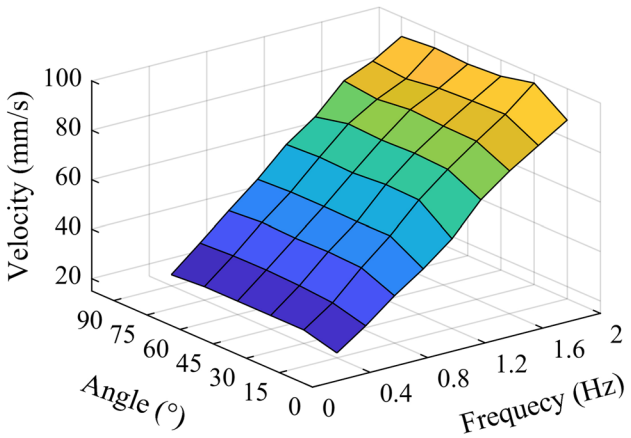

Fig. 25 The velocity of the robot prototype at different frequency and deflecting angle

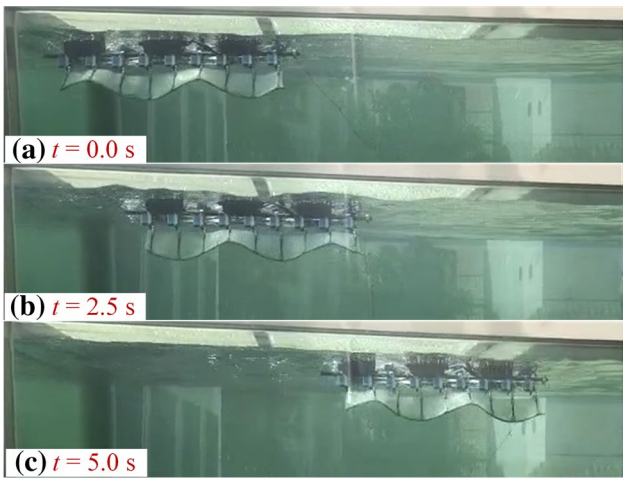

Fig. 26 The underwater forward motion images of the robot prototype, frequency = 2.0 Hz

4.3 Swimming Experiment

Underwater experiments are carried out in an outdoor tank with 4 m long, 2 m width, and 2 m height. The forward motion and backward motion have been realized, respectively, when the wave propagation direction is set as the opposite. Figure 26 presents the underwater motion images of the robot prototype when the frequency is 2.0 Hz. The results show that the undulating fins could achieve stable wave transmission. Under the thrust provided by the undulatory propellers, the robot accelerated first and then reached to the maximum speed. During the cruise movement, the robot presented good stability and low noise. And there is almost no water flower around the robot, which proves that the propulsion of bionic undulatory fin has an advantage in environmental adaptivity and concealment.

Furthermore, we tested the swimming velocity at different undulating frequency. As shown in Fig. 27, with the increase of frequency, the swimming speed of the robot gradually increases; and the maximum speed is about 0.31 m/s when the frequency is 2.0 Hz. As undulating frequency is limited by the driving ability of servo motors, motors with higher velocity are needed to further improve the robot's swimming speed.

4.4 Cross-media Experiment

The experiments in single media have revealed that the robot can realize both land and underwater locomotion by the same undulating propeller. For amphibious robot, one of the most important evaluation targets is land–water switching capability, which is used to be quite complex, because traditional amphibious robots usually use two driven systems and they need to switch propulsion mechanism in different media. However, it is easy for the bionic amphibious robot to achieve continuous transmission owing to the same propulsion of the undulatory propeller. To verify the robot adaptivity in waterfront environment, we tested the motion of the robot near a field river. As shown in Fig. 28, the robot first moved forward in the sand road and transmitted into the water. Finally, it successfully submerged and swam underwater. The cross-media experiment achieved the integrated drive of the undulating fin propelled robot.

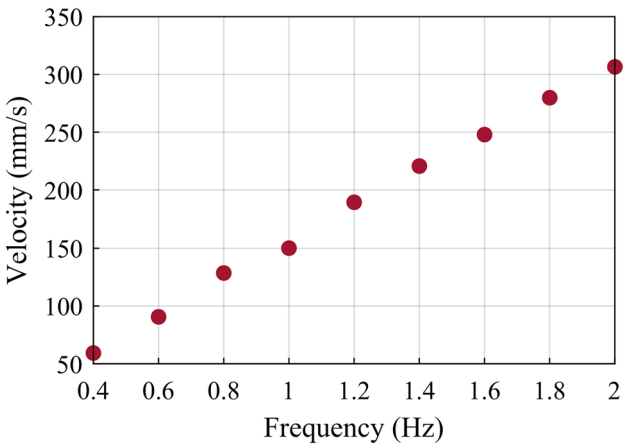

Fig. 27 The relationship of the swimming velocity and undulating frequency

5 Discussion

Based on the theoretical analysis, virtual simulation and prototype experiments, the newly designed undulating fin, and the amphibious robot were proved to be feasible and practical. The performance and characteristics are discussed below in terms of structure, materials, actuation, locomotion capacities, and possible improvement.

(1) Bionic structure: Compared to natural creatures propelled by medium or pectoral fins which are generally composed of more than 200 fin rays [37], bionic mechanical fins often suffer from incomplete wave and internal stress because of limited fin rays. However, it is accompanied with more complex structure and control strategy when increasing the number of fin rays. To address this issue, we improved the conventional undulating fin propulsor by initializing the membrane fin as a standard sine-wave shape; and the fin is equipped with multiple three-degree-of-freedom fin ray unit. As a result, the membrane fin can always keep a perfect sine-wave shape in the whole process of wave propagation. To extend the movement of the undulating fin to an amphibious space, we combined the flexible fin with a bending spring, which balanced the contradictory demands of flexibility and rigidity. Those specially designed mechanisms made the soft amphibious fin more practical, more flexible, and more bionic.

(2) Materials and weight: The undulating fin should be as light and soft as possible so as to reduce driven load for amphibious robot. However, it should also be heavy and rigid enough to ensure carrying capacity on land, which is not necessary for conventional underwater

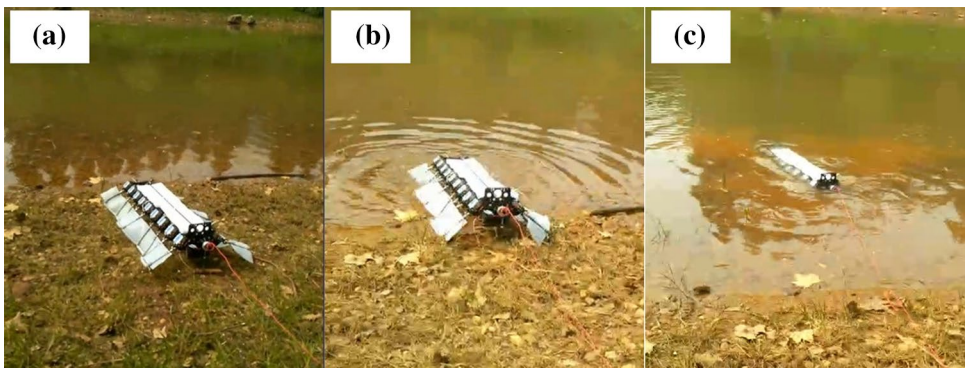

Fig. 28 The motion images during cross-media experiment of the amphibious robot

robotic fin. These contradictory demands make it difficult to find the proper materials and parameters for the undulating fin. On the other hand, the friction with the ground will cause wear and damage of the undulating fin, which also increases material cost. Compared to the existing mechanical fins which fabricate the undulating fin as a whole, our combination of flexible fin and rigid bending spring solves these problems, because the fin does not need to touch the ground. And the spring, instead of the fin, acts as the load bearing part. Therefore, the underwater undulating fin can be used directly for terrestrial case. We choose silica gel (2 mm) for the flexible fin and metal for structural parts. Considering the three-dimensional size, the weight of our robot prototype is only 4.75 kg and the mechanical fin weighs only 0.97 kg. In addition, the undulating fin interacts with the ground via rubber tubes which are easy to replace, making the fin more durable and reliable.

(3) Composite wave-driven mechanics: For engineering realization, the fin ray of bionic undulating fin in the existing studies has only one-degree-of-freedom, i.e., it can only oscillate up and down around the baseline of undulating fin. However, the natural fins have multiple degrees of freedom to form more kinds of waveforms for more complex movements. In this paper, we use a self-adaptive fin ray unit which has other two passive rotational freedom for better effect. The dual interaction of the elastic steel slice and the bending spring gives the undulating fin a freedom to oscillate back and forth along the fin baseline, thus forming a passive longitudinal wave. This composite wave causes the undulating fin to output a modulated waveform. The theoretical analysis and the simulation results prove that this composite wave improves land walking compared to single transverse wave. This new composite wave-driven method is expected to improve driving performance and walking speed of amphibious undulating fin in the future.

(4) Locomotion capacities: The experiments show that the robot prototype can walk forward, backward, and steering in a variety of terrains. And it can swim underwater. In addition, the robot can also cross between water and land. All these locomotion relies on the same undulating motion. Owning to this integrated driven system, the robot does not need to switch propulsion mechanism, thus reducing both the mechanical complexity and control complexity. Compared to the conventional amphibious robot using wheels or tracks on land and propellers or jets underwater, the undulating propulsor improves the reliability and adaptability of the robot.

6 Conclusion and Future Work

As the traditional amphibious robots often use two prolusion systems and need to switch manually in different environment, we are motivated to develop a united driven system so as to reduce the structure complexity and enhance system reliability. Borrowing the propulsion method of fishes and snakes, a bionic amphibious undulating fin propulsor has been developed in this paper. The whole work is concluded as below.

(1) To address the issue that the flexible fin should be both flexible enough for aquatic medium and rigid enough for terrestrial medium, we use a special combination of a membrane-like fin and a bending spring. A self-adaptive oscillating unit with two passive rotational degree of freedom is designed to reduce resistance and internal forces. Since the bending spring is not easy to be stretched, a sheet of spring steel is used as the connect to the fin ray, which therefore can oscillate passively at horizontal direction while being actuated up and down. Besides, we have proposed a method to make amphibious undulating fin by straightening an arc-shaped sheet so as to maintain sinusoidal shape.

(2) The dynamic model of the undulating fin is established and locomotion process is analysed. We have got a qualitative conclusion that there is a passively generated longitudinal wave while the transverse wave propagates. The passive longitudinal wave is periodic and results in relative motion to the ground so drives the robot moving forward.

(3) To explore the locomotion mechanism of the compound waves, a virtual prototype in ADAMS software has been established and simulation is conducted. The results show that the longitudinal wave is also a sine wave, and its frequency is twice that of the transverse wave. The interaction of the composite waves contributes to the locomotion of the robot.

(4) An amphibious robot prototype actuated by a pair of undulatory fin propulsors has been developed. Manoeuvrability has been verified in land, water and cross-media experiments, thus giving evidence to the feasibility of the newly designed undulating fin for amphibious locomotion.

Although the novel bionic amphibious fin achieves basic motion, the robots can be improved in some aspects. For example, it is necessary to build a more accurate dynamic model for the space motion of the robot. At the same time, buoyancy adjustment and gravity centre adjustment devices can be introduced for multi-mode locomotion. The

control algorithm can also be updated for precise attitude and depth control.

Supplementary Information The online version contains supplementary material available at https://doi.org/10.1007/s42235-022-00328-4.

Acknowledgements This research is supported by the National Natural Science Foundation of China (Grant No. 52075537 and Grant No. 52105289).

Data Availability Statement The datasets generated during and/or analysed during the current study are available from the corresponding author on reasonable request.

Declarations

Conflict of Interest The authors declare that there is no conflict of interest.

References

1. Baines, R. L., Fish, F. E., & Kramer-Bottiglio, R. (2020). Amphibious robotic propulsive mechanisms: Current technologies and open challenges. In: D. A. Paley & N. M. Wereley (Eds.), *Bioinspired Sensing, Actuation, and Control in Underwater Soft Robotic Systems* (pp. 41–69). Springer.
2. Rafeeq, M., Toha, S. F., Ahmad, S., & Razib, M. A. (2021). Locomotion strategies for amphibious robots-a review. *IEEE Access, 9*, 26323–26342.
3. Bai, X. J., Shang, J. Z., Luo, Z. R., Jiang, T., & Yin, Q. (2022). Development of amphibious biomimetic robots. *Journal of Zhejiang University-Science A, 23*(3), 157–187.
4. Wu, Z. Y., Qi, J., & Zhang, S. (2014). Amphibious robots: A review. *Applied Mechanics and Materials, 494–495*, 1036–1041.
5. Ren, K., & Yu, J. C. (2021). Research status of bionic amphibious robots: A review. *Ocean Engineering, 227*(8), 108862.
6. Guo, Z. Y., Li, T., & Wang, M. L. (2018). A survey on amphibious robots. In: 2018 37*th Chinese Control Conference (CCC)* (pp. 185–190). Wuhan, China.
7. Altendorfer, R., Moore, N., Komsuoglu, H., Buehler, M., Brown, H. B., Mcmordie, D., Saranli, U., Full, R. J., & Koditschek, D. E. (2001). Rhex: A biologically inspired hexapod runner. *Autonomous Robots, 11*(3), 207–213.
8. Johnson, A. M, & Koditschek, D. E. (2013). Toward a vocabulary of legged leaping. In: *IEEE International Conference on Robotics & Automation (ICRA)* (pp. 2568–2575). Karlsruhe, Germany.
9. Boxerbaum, A. S., Werk, P., Quinn, R. D., & Vaidyanathan, R. (2005). Design of an autonomous amphibious robot for surf zone operation: Part i mechanical design for multi-mode mobility. In: *IEEE/ASME International Conference on Advanced Intelligent Mechatronics* (pp. 1459–1464). California, USA.
10. Harkins, R., Ward, J. L., Vaidyanathan, R., Boxerbaum, A. S., & Quinn, R. D. (2005). Design of an autonomous amphibious robot for surf zone operations: Part ii - hardware, control implementation and simulation. In: *IEEE/ASME International Conference on Advanced Intelligent Mechatronics* (pp. 1465–1470). California, USA.
11. Zhang, S. W., Zhou, Y. C., Xu, M., Liang, X., Liu, J. M., & Yang, J. (2016). AmphiHex-I: Locomotory performance in amphibious environments with specially designed transformable flipper legs. *IEEE/ASME Transactions on Mechatronics, 21*, 1720–1731.
12. Greiner, H., Shectman, A., Won, C., Elsley, R. E., & Beith, P. (1996). Autonomous legged underwater vehicles for near land warfare. *Symposium on Autonomous Underwater Vehicle Technology* (pp. 41–48). Monterey, USA.
13. Yoo, S., Shim, H., Jun, B., Park, J., & Lee, P. (2016). Design of walking and swimming algorithms for a multi-legged underwater robot crabster cr200. *Marine Technology Society Journal, 50*(5), 74–87.
14. Wang, L. Q., Wang, H. L., Wang, G., Chen, X., Khan, A., & Jin, L. X. (2018). Investigation of the hydrodynamic performance of crablike robot swimming leg. *Journal of Hydrodynamics, 30*, 605–617.
15. Ayers, J. (2004). Underwater walking. *Arthropod Structure & Development, 33*(3), 347–360.
16. Kato, N. (2011). Swimming and walking of an amphibious robot with fin actuators. *Marine Technology Society Journal, 45*(4), 181–197.
17. Shi, L. W., Guo, S. X., Mao, S. L., Yue, C. F., Li, M. X., & Asaka, K. (2013). Development of an amphibious turtle-inspired spherical mother robot. *Journal of Bionic Engineering, 10*(4), 446–455.
18. Song, S., Kim, M., Rodrigue, H., Lee, J., Shim, J., Kim, M., Chu, W., & Ahn, S. (2016). Turtle mimetic soft robot with two swimming gaits. *Bioinspiration & Biomimetics, 11*, 036010.
19. Ijspeert, A. J., Crespi, A., Ryczko, D., & Cabelguen, J. (2007). From swimming to walking with a salamander robot driven by a spinal cord model. *Science, 315*(5817), 1416–1420.
20. Fan, J. Z., Zhang, W., Kong, P. C., Cai, H. G., & Liu, G. F. (2017). Design and dynamic model of a frog-inspired swimming robot powered by pneumatic muscles. *Chinese Journal of Mechanical Engineering, 30*(5), 1123–1132.
21. Paschal, T., Bell, M. A., Sperry, J., Sieniewicz, S., Wood, R. J., & Weaver, J. C. (2019). Design, fabrication, and characterization of an untethered amphibious sea urchin-inspired robot. *IEEE Robotics and Automation Letters, 4*(4), 3348–3354.
22. Ohashi, T., Yamada, H., & Hirose, S. (2010). Loop forming snake-like robot acm-r7 and its serpenoid oval control. In: *IEEE/RSJ International Conference on Intelligent Robots & Systems* (pp. 413–418). Taipei, Taiwan.
23. Yu, S. M., Wang, M. H., Ma, S. G., Li, B., & Wang, Y. C. (2012). Development of an amphibious snake-like robot and its gaits on ground and in water. *Journal of Mechanical Engineering, 48*(9), 18.
24. Yu, J. Z., Ding, R., Yang, Q. H., Tan, M., Wang, W. B., & Zhang, J. W. (2012). On a bio-inspired amphibious robot capable of multimodal motion. *IEEE/ASME Transactions on Mechatronics, 17*, 847–856.
25. Filardo, B. P., Zimmerman, D. S., & Weaker, M. I. (2020). Vehicle with traveling wave thrust module apparatuses, methods and systems. US20200149555A1. https://patents.justia.com/patent/11209022, https://www.freepatentsonline.com/y2020/0149555.html.
26. Sfakiotakis, M., Lane, D. M., & Davies, J. B. (1999). Review of fish swimming modes for aquatic locomotion. *IEEE Journal of Oceanic Engineering, 24*(2), 237–252.
27. Sfakiotakis, M., Lane, D. M., & Davies, B. C. (2001). An experimental undulating-fin device using the parallel bellows actuator. In: *IEEE International Conference on Robotics and Automation (ICRA)* (pp. 2356–2362). Seoul, South Korea.
28. Curet, O. M., Patankar, N. A., Lauder, G. V., & Maciver, M. A. (2011). Mechanical properties of a bio-inspired robotic knifefish with an undulatory propulsor. *Bioinspiration & Biomimetics, 6*(2), 026004.
29. Low, K. H., & Willy, A. (2006). Biomimetic motion planning of an undulating robotic fish fin. *Journal of Vibration & Control, 12*(12), 1337–1359.
30. Rahman, M. M., Sugimori, S., Miki, H., Yamamoto, R., Sanada, Y., & Toda, Y. (2013). Braking performance of a biomimetic squid-like underwater robot. *Journal of Bionic Engineering, 10*, 265–273.

31. Wei, Q. P., Wang, S., Dong, X., Shang, L. J., & Tan, M. (2013). Design and kinetic analysis of a biomimetic underwater vehicle with two undulating long-fins. *Acta Automatica Sinica, 39*(8), 1330–1338.
32. Liu, H., & Curet, O. M. (2018). Swimming performance of a bio-inspired robotic vessel with undulating fin propulsion. *Bioinspiration & Biomimetics, 13*, 056006.
33. Li, Y. X., Chen, L. G., Wang, Y., & Ren, C. (2021). Design and experimental evaluation of the novel undulatory propulsors for biomimetic underwater robots. *Bioinspiration & Biomimetics, 16*, 056005.
34. Sfakiotakis, M., Gliva, R., & Mountoufaris, M. (2016). Steering-plane motion control for an underwater robot with a pair of undulatory fin propulsors. In: 2016 24*th Mediterranean Conference on Control and Automation (MED)* (pp. 496–503). Athens, Greece.
35. Low, K. H., Zhou, C. L., Seet, G., Bi, S. S., & Cai, Y. R. (2012). Improvement and testing of a robotic manta ray (RoMan-III). In: *IEEE International Conference on Robotics and Biomimetics (ROBIO)* (pp. 1730–1735). Phuket, Thailand.
36. Wang, S., Wang, Y., Wei, Q. P., Tan, M., & Yu, J. Z. (2017). A bio-inspired robot with undulatory fins and its control methods. *IEEE/ASME Transactions on Mechatronics, 22*(1), 206–216.
37. Hu, T. J., Li, F., Wang, G. M., & Shen, L. C. (2005). Morphological measurement and analysis of gymnarchus niloticus. *Journal of Bionic Engineering, 2*, 25–31.